Computers & Geosciences 98 (2017) 1–8

Contents lists available at ScienceDirect

Computers & Geosciences

journal homepage: www.elsevier.com/locate/cageo

Research paper

Variational-based segmentation of bio-pores in tomographic images

Benjamin Bauer[a], Xiaohao Cai[b], Stephan Peth[c], Katja Schladitz[a,*], Gabriele Steidl[d]

[a] Fraunhofer ITWM, Department of Image Processing, Kaiserslautern, Germany
[b] University of Cambridge, Department of Plant Sciences, and Department of Applied Mathematics and Theoretical Physics, UK
[c] University of Kassel, Department of Soil Science, Germany
[d] University of Kaiserslautern, Department of Mathematics, Germany

ARTICLE INFO

Keywords:
3D image segmentation
Bio-pores
Root system
Variational segmentation
Total variation minimization
Gray value thresholding
Morphological segmentation

ABSTRACT

X-ray computed tomography (CT) combined with a quantitative analysis of the resulting volume images is a fruitful technique in soil science. However, the variations in X-ray attenuation due to different soil components keep the segmentation of single components within these highly heterogeneous samples a challenging problem. Particularly demanding are bio-pores due to their elongated shape and the low gray value difference to the surrounding soil structure.

Recently, variational models in connection with algorithms from convex optimization were successfully applied for image segmentation. In this paper we apply these methods for the first time for the segmentation of bio-pores in CT images of soil samples. We introduce a novel convex model which enforces smooth boundaries of bio-pores and takes the varying attenuation values in the depth into account. Segmentation results are reported for different real-world 3D data sets as well as for simulated data. These results are compared with two gray value thresholding methods, namely indicator kriging and a global thresholding procedure, and with a morphological approach. Pros and cons of the methods are assessed by considering geometric features of the segmented bio-pore systems. The variational approach features well-connected smooth pores while not detecting smaller or shallower pores. This is an advantage in cases where the main bio-pores network is of interest and where infillings, e.g., excrements of earthworms, would result in losing pore connections as observed for the other thresholding methods.

1. Introduction

Computed tomography (CT) is an efficient tool for non-destructive imaging and the subsequent analysis of the structure of plant roots, see Mooney (2002), Tracy et al. (2010) and the references therein. Although the quality of CT images in soil science has rapidly improved in recent years, the segmentation of bio-pores remains a challenging problem. This is mainly due to the overlap of the X-ray attenuation values between bio-pores and soil caused by organic materials, and the elongated shape of the pores. Especially it appears if the pores contain partly decomposed root fragments or earthworm linings. Such features are only temporarily occupying the bio-pores and it may be desired to omit them from the segmented bio-pore network for a separate analysis. Fig. 1(a) shows exemplary a three-dimensional (3D) CT image of soil with bio-pores.

The accurate segmentation of the bio-pores is of substantial interest since the appropriate segmentation is a key determinant for the quality of the subsequent structural analysis. For example, disconnecting bio-pores due to poor segmentation can influence the subsequent analysis of the bio-pore network dramatically. It may also be of interest to exclude temporal features such as earthworm infillings from the segmented images to be able to analyse bio-pore features such as surface to volume ratios or network geometries independently.

In Pagenkemper et al. (2013), CT was used to investigate the effects of root-induced bio-pores on the pore space of soil samples. These pore spaces are made up of a variety of different pore types showing structural heterogeneity in size, shape, and orientation. Methods relying on local or global gray value thresholds have been successfully applied to segment different pore systems as, e.g., Oh's and Lindquist's indicator kriging (Oh and Lindquist, 1999) in Pagenkemper et al. (2013) or a refined version of the double thresholding (Vogel and Kretzschmar, 1996) in Schlüter et al. (2010). For a comparison of these and some other methods for the segmentation of porous materials we refer to Iassonov et al. (2009) and for those of (multiphase) soil images with macro-pores, organic matter and rocks to Schlüter et al. (2014).

In this paper, we suggest a novel variational model for segmenting large root channels. It consists of two ingredients: a *data term* which includes a threshold depending on the depth (z-direction) of the given

* Corresponding author.
E-mail address: katja.schladitz@itwm.fraunhofer.de (K. Schladitz).

http://dx.doi.org/10.1016/j.cageo.2016.09.013
Received 1 June 2015; Received in revised form 1 June 2016; Accepted 30 September 2016
Available online 03 October 2016
0098-3004/

data and takes the illumination/attenuation changes in this direction into account, and a *regularizing term* which is a discrete counterpart of the total variation function (Rudin et al., 1992) and takes care of smooth boundaries of the bio-pores.

Approaches for the denoising and segmentation of images based on the calculus of variation have been applied very successfully in recent years. Among the most influential examples are the Rudin-Osher-Fatemi total-variation based image denoising model (Rudin et al., 1992) and the Mumford-Shah (MS) model image segmentation model (Mumford and Shah, 1989). The MS model supports smooth image segments with small boundary lengths. Since the MS model is neither convex nor smooth, it is hard to find a global minimizer numerically. The simpler piecewise constant MS model focuses on piecewise constant segments. For the two phase segmentation this model is actually the active contour model of Chan and Vese (2001) which is still non convex. Several convex relaxations of the piecewise constant supervised model were proposed in the literature, also for multiphase case, see, e.g., Lellmann et al. (2009), Nikolova et al. (2006), Pock et al. (2009), Zach et al. (2008). These models have the advantage that they have only global minima which can be computed by standard convex minimization schemes. For the two phase segmentation it was shown in Nikolova et al. (2006) that the above convex relaxed approaches find the global minimum of the original non convex model. Our proposed model can be considered as a modification of these convex approaches which takes illumination changes via a special data term into account. For a very recent comprehensive study of energy minimizing methods for the segmentation of natural images we refer to Kappes et al. (2015).

We suggest to find the global minimizer of our convex model by the alternating direction method of multipliers (ADMM) (Boyd et al., 2011; Gabay, 1983) which has a simple implementation and works very efficiently.

We compare our variational method with three other usual segmentation approaches. More precisely, we apply indicator kriging (Oh and Lindquist, 1999) as used in Pagenkemper et al. (2013), a global gray value thresholding (Otsu, 1979), and a morphological extract holes procedure combined with a global thresholding. All these methods require, in contrast to the variational method, some pre- and postprocessing steps described in Section 3 which handle in particular the illumination changes in the z-direction. All four methods are applied to four data sets from Pagenkemper et al. (2013) and to two simulated data sets. Quantitative assessment of the segmented pores shows that each method has its merits. The variational approach yields smooth well-connected large pores. Non detection of smaller or shallower pores can be an advantage in cases where the main bio-pores network is of interest. Moreover, the smooth surface eases subsequent skeletonization as artificial branches due to local surface roughness are avoided. On the other hand, morphological correction of global gray value fluctuations followed by a simple global gray value thresholding according to Otsu (1979) very well recovers small pores and biological infillings.

This paper is organized as follows: In Section 2, we introduce our variational model for segmenting 3D root-induced bio-pores and propose an efficient ADMM algorithm to find the global minimizer. The segmentation methods used for the comparison are shortly summarized in Section 3. In Section 4, we test our algorithm on four 3D image data sets from Pagenkemper et al. (2013) as well as on two simulated bio-pore systems and compare it to the segmentation algorithms introduced in the previous section. Conclusions are given in Section 5.

2. Variational segmentation model

In this section, we introduce our model for tackling the root-induced bio-pores segmentation problem and provide an algorithm to solve it.

Let $\Omega := \{1, \ldots, N_1\} \times \{1, \ldots, N_2\} \times \{1, \ldots, N_3\}$ be the image grid. For fixed $z \in \{1, \ldots, N_3\}$, let $\Omega_z := \{(x, y, z): (x, y) \in \{1, \ldots, N_1\} \times \{1, \ldots, N_2\}\}$ be the horizontal (discrete) plane through z. By $f: \Omega \to [0, 1]$ we denote the given 3D CT gray-value image. Let ∇_x be the forward difference operator in x-direction (and similarly in y- and z-direction), i.e.,

$$\nabla_x f(x, y, z) := f(x + 1, y, z) - f(x, y, z),$$

where we suppose mirror boundary conditions. For fixed $z \in \{1, \ldots, N_3\}$ and given $\varepsilon > 0$ we define the edge set $\mathcal{E}_z(\varepsilon) \in \Omega_z$ by

$$\mathcal{E}_z(\varepsilon) := \{(x, y) \in \Omega_z: \sqrt{(\nabla_x f(x, y, z))^2 + (\nabla_y f(x, y, z))^2} > \varepsilon\}.$$

In other words, $\mathcal{E}_z(\varepsilon)$ contains the voxels located around the boundaries in Ω_z. Then

$$\phi(z) := \frac{1}{|\mathcal{E}_z(\varepsilon)|} \sum_{(x,y) \in \mathcal{E}_z(\varepsilon)} f(x, y, z) \tag{1}$$

can be considered as average gray value of the voxels located around the boundaries in Ω_z. We define a threshold function τ depending on z by

$$\tau(z) := c + \phi(z), \tag{2}$$

where c is a chosen constant. To segment the root-induced bio-pores we propose to find the minimizer u of the convex functional

$$\min_{u \in [0,1]} \sum_{(x,y,z) \in \Omega} \underbrace{(\tau(z) - f(x, y, z))}_{s(x,y,z)} u(x, y, z) + \mu TV(u), \quad \mu > 0, \tag{3}$$

where $u \in [0, 1]$ is meant voxelwise and

$$TV(u) := \sum_{(x,y,z) \in \Omega} \sqrt{(\nabla_x u(x, y, z))^2 + (\nabla_y u(x, y, z))^2 + (\nabla_z u(x, y, z))^2}.$$

The first term of model (3) is a data term. If $f(x, y, z)$ is larger or equal than the threshold $\tau(z)$, then a large $u(x, y, z) \approx 1$ is not penalized. Conversely, if $f(x, y, z)$ is below the threshold, then the data term becomes small for $u(x, y, z) \approx 0$. The second term is the regularization term which imposes smooth boundaries. In particular small image details (artifacts) are neglected. This well-known regularizing term was first introduced by Rudin et al. (1992) for image restoration tasks, The data and the regularization terms are coupled by the regularization parameter μ which steers the influence of the different terms to the solution. Note that due to the attenuation values between bio-pores at different z layers, a layer adapted value $\tau(z)$ leads to better segmentation results.

There is a close relation of model (3) (for constant τ) to the Chan-Vese segmentation model (Chan and Vese, 2001). For more details on the connection between these models and its relation to perimeter minimization we refer to Cai and Steidl (2013), Chambolle et al. (2010).

Once the minimizer $u: \Omega \to [0, 1]$ of (3) is found, we can apply a thresholding procedure with a threshold $\rho \in (0, 1)$ to find the two desired segments of u. Fortunately it was proved in Nikolova et al. (2006) that every threshold $\rho \in (0, 1)$ can be used here.

We compute the minimizer of the convex functional (3) by the ADMM (Boyd et al., 2011; Gabay, 1983). Alternatively one could apply primal-dual first order methods as, e.g., those proposed in Chambolle and Pock (2011). To present the algorithm in a sound mathematical form, we reorder the 3D images $g: \Omega \to \mathbb{R}$ into vectors $g \in \mathbb{R}^N$, $N = N_1 N_2 N_3$ with components $g_{x+N_1(y-1)+N_1N_2(z-1)} := g(x, y, z)$ and associate to the forward difference operators ∇_x, ∇_y, ∇_z the corresponding matrices. For the concrete matrix representation we refer to Shafei and Steidl (2012). Then problem (3) can be rewritten as

$$\min_{u,v,w} \langle s, u \rangle + \mu \| \sqrt{v_x^2 + v_y^2 + v_z^2} \|_1 \quad \text{subject to } v = \nabla u, \; w = u, \; w \in [0, 1],$$

where $\langle s, u \rangle$ denotes the vector inner product, $\|\cdot\|_1$ the 1-norm of vectors and

$$\nabla = \begin{pmatrix} \nabla_x \\ \nabla_y \\ \nabla_z \end{pmatrix}, \quad v := \begin{pmatrix} v_x \\ v_y \\ v_z \end{pmatrix}.$$

Then the ADMM algorithm reads as follows:

algorithm 1. .

Initialization: $v^{(0)} \in \mathbb{R}^{3N}$, $w^{(0)} \in \mathbb{R}^N$, $b_1^{(0)} \in \mathbb{R}^{3N}$, $b_2^{(0)} \in \mathbb{R}^N$, and $\gamma > 0$.
Iterations: For $r = 0, 1, \ldots$

$u^{(r+1)} = \operatorname{argmin}_u \{\langle s, u\rangle + \frac{\gamma}{2} \| \nabla u - v^{(r)} + b_1^{(r)} \|_2^2 + \frac{\gamma}{2} \| u - w^{(r)} + b_2^{(r)} \|_2^2\}$

$v^{(r+1)} = \operatorname{argmin}_v \{\mu \| v \|_1 + \frac{\gamma}{2} \| \nabla u^{(r+1)} - v + b_1^{(r)} \|_2^2\}$

$w^{(r+1)} = \operatorname{argmin}_{w \in [0,1]} \| u^{(r+1)} - w + b_2^{(r)} \|_2^2$

$b_1^{(r+1)} = b_1^{(r)} + u^{(r+1)} - v^{(r+1)}$

$b_2^{(r+1)} = b_2^{(r)} + u^{(r+1)} - w^{(r+1)}$

The minimizer in the first step can be computed by setting the gradient to zero which results in solving the linear system of equations

$$(\nabla^T \nabla + I_N) u^{(r+1)} = \nabla^T (v^{(r)} - b_1^{(r)}) + (w^{(r)} - b_2^{(r)}) - \frac{1}{\gamma} s$$

with the $N \times N$ identity matrix I_N. This system can be efficiently solved using the fast discrete cosine transform, see Shafei and Steidl (2012). The second step requires a grouped soft shrinkage of $a = (a_1, a_2, a_3)^T := \nabla u^{(r+1)} + b_2^{(r)}$ with threshold $\lambda := \frac{\mu}{\gamma}$ defined voxelwise for $k = 1, 2, 3$ by

$$v_k^{(r+1)} = \begin{cases} a_k \left(1 - \frac{\lambda}{\sqrt{a_1^2 + a_2^2 + a_3^2}}\right) & \text{if } \sqrt{a_1^2 + a_2^2 + a_3^2} > \lambda, \\ 0 & \text{otherwise.} \end{cases}$$

The third step just means that

$$w^{(r+1)} = \min\{\max\{0, u^{(r+1)} + b_2^{(r)}\}, 1\}.$$

3. Segmentation methods for comparison

In order to evaluate the derived segmentation algorithm, we compare it with

i) the indicator kriging method (IK) (Oh and Lindquist, 1999) as used in Pagenkemper et al. (2013),
ii) a global thresholding according to Otsu (1979), and
iii) a morphological approach thriving mainly on the extract-holes transform on gray value images (Soille, 1999).

Every method comes along with some pre- and postprocessing steps. To be self-consistent we briefly summarize the three methods. All three methods described here thrive on global gray value thresholding. For the present data this straightforward approach is however prevented by strong global gray value variations. Therefore, a global gray value balancing (shading/illumination correction) is applied as follows: First we correct slicewise, for each slice perpendicular to the z-axis (height of the cylindrical sample). More precisely, let $\overline{m}$ denote the global gray value mean of the cylindrical sample C, and

$$m(z) := \frac{1}{\#(\Omega_z \cap C)} \sum_{(x,y) \in (\Omega_z \cap C)} f(x, y, z)$$

the gray value mean of the slice at height z. The corrected gray values are then given as

$$f_{corr}(x, y, z) = f(x, y, z) + \overline{m} - m(z).$$

For the second shading correction, the image is transformed in cylindrical coordinates such that the radius is mapped to the z-coordinate. Subsequently, the above described slicewise shading correction is applied in the new coordinate system. Finally, the corrected gray values are mapped back to the original image.

3.1. Indicator kriging

The backbone of the method applied in Pagenkemper et al. (2013) is indicator kriging. In user defined regions of interest, two thresholds $T_0 \le T_1$ are derived from the data. Voxels darker than T_0 are assigned to the pore space, while voxels brighter than T_1 are assigned to the solid component. The decision for voxels x with $T_0 < f(x) < T_1$ is taken according to an iterative procedure adapted from the geostatistical interpolation method kriging that takes into account the local gray value distribution in the image via the covariance function. The quality of the segmentation result is strongly determined by the choice of the two thresholds as only a comparably small number of voxels is later assigned using the actual indicator kriging procedure. In Pagenkemper et al. (2013), the threshold T_1 is chosen as the global gray value mean minus 2σ, where σ is the standard deviation of the Gaussian fit to the matrix peak. The local lower threshold T_0 is the bio-pore gray value peak for the manually chosen region.

3.2. Global thresholding according to Otsu

The simplest method is global thresholding with an automatically chosen threshold T. For the data considered here, this can only be applied to the illumination corrected image as described above. We use Otsu's method (Otsu, 1979) to determine T: Assuming a bimodal gray value distribution, Otsu's threshold is the one maximizing the intra-class variance of the two gray value classes while minimizing the gray value variances within the two classes.

3.3. Morphological approach via extract-holes transform

As an alternative, the morphological extract holes transform (Soille, 1999) is applied to the shading corrected data. That is, the same morphological correction for global gray value fluctuations as above has been applied. Holes in an integer gray value image are regional gray value minima not connected to the image borders. Regional minima in turn are connected regions of voxels of constant gray value such that any path to a voxel of a lower gray value includes at least one voxel of a higher gray value. Extract holes results in an integer image of the holes and everything else is background. We finally apply Otsu's threshold to this image to segment the pore system.

4. Experimental results

In this section, we compare the novel variational method with the segmentation results achieved by the three methods reported in the previous section.

The variational segmentation method was implemented in Matlab. The program code is available at http://www.mathematik.uni-kl.de/imagepro/software/. To process a 3D data with size $399 \times 399 \times 983$, the time cost of the variational method introduced in the paper is less than one hour ($\le$100 iterations of ADMM) on a workstation with 2. 4 GHz processor and 50 GB RAM. For all other processing and analysis algorithms as well as the volume rendering we used MAVI (Fraunhofer ITWM, 2005) and ToolIP Fraunhofer ITWM (2009) with MAVIkit Fraunhofer ITWM (2013).

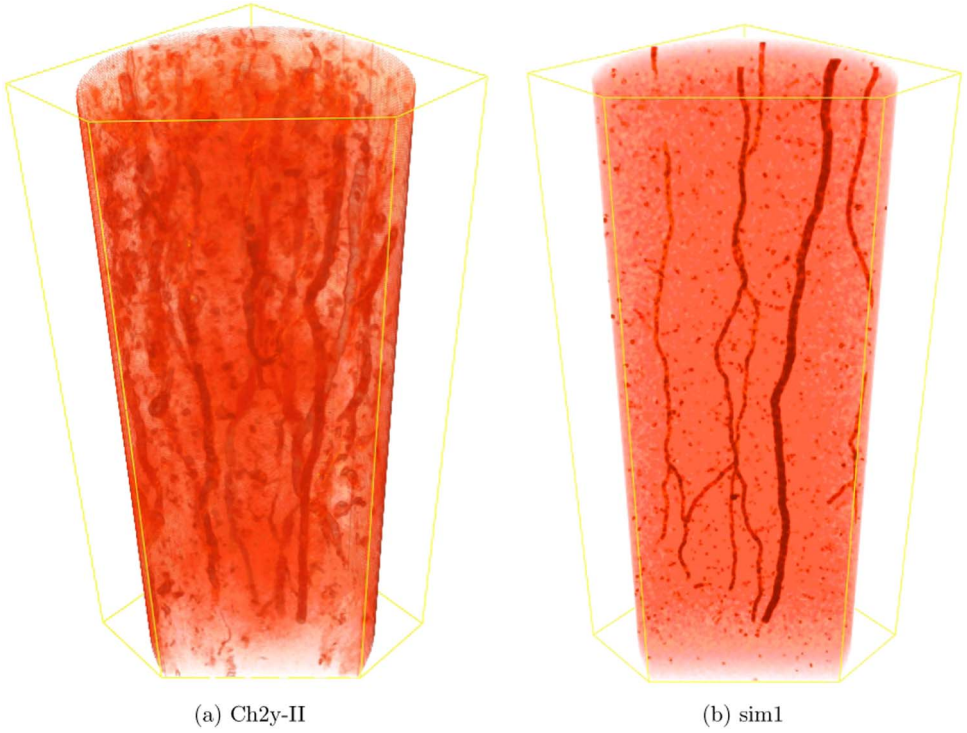

Fig. 1. Volume renderings of the tomographic image of the soil sample Ch2y-II from Pagenkemper et al. (2013) and of a simulated soil sample used later on for algorithm validation. Ch2y-II was imaged with a voxel size of 463 μm at the Technical University Dortmund, Germany, Department of Mechanical Engineering with a vltomelx 240 (Phoenix-X-Ray). For details on sample preparation and imaging parameters see Pagenkemper et al. (2013). The rendering shows 399 × 399 × 983 voxels corresponding to 185 mm × 185 mm × 455 mm. (a) Ch2y-II (b)sim1.

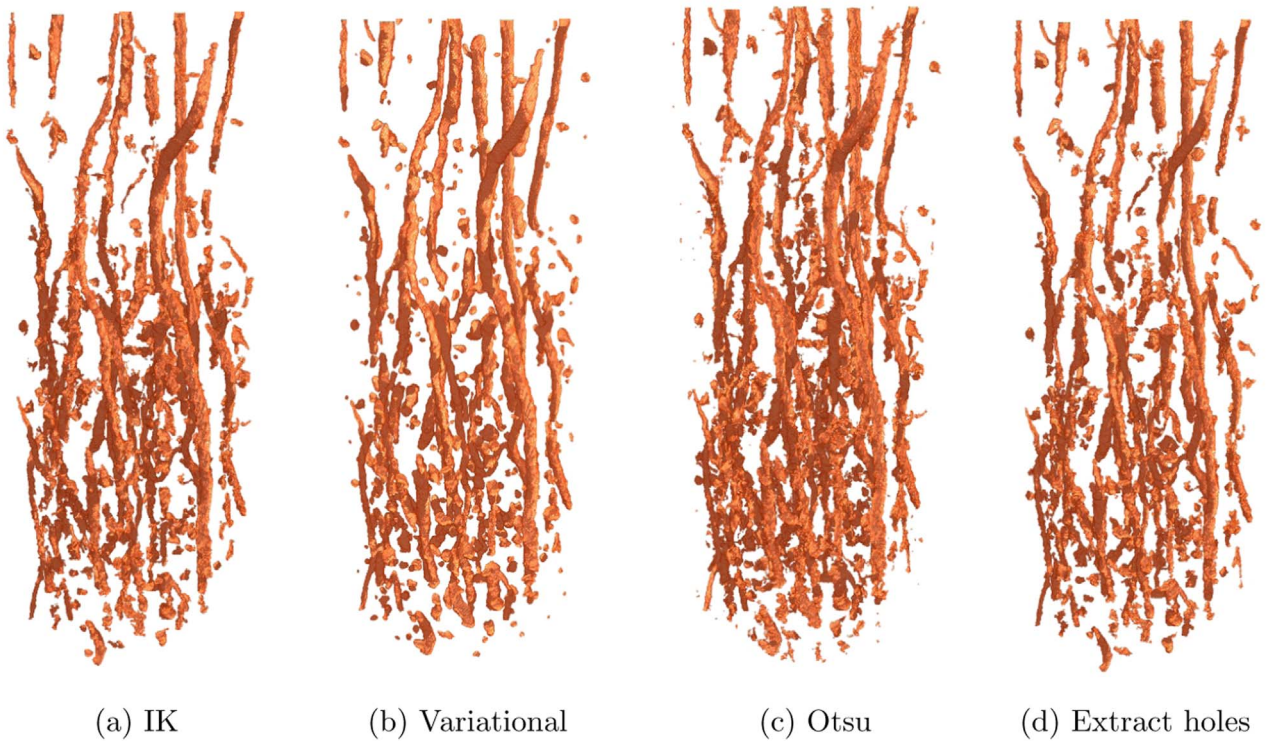

Fig. 2. 3D rendering of the segmentation results for Ch2y-II after removing all objects smaller than 800 voxels. (a)IK (b)Variational (c)Otsu (d)Extract holes.

4.1. Data sets

For the evaluation we use four different data sets from Pagenkemper et al. (2013), where more information on the data can be found. We have one monolith of fescue (Fe1y) after two years, two monoliths of alfalfa (Af2y) after one, resp. two years and one monolith of chicory (Ch2y) after two years of undisturbed cultivation. Fescue as a shallow rooter represents a bio-pore poor treatment that should not generate bio-pores in the subsoil. On the contrary, alfalfa and chicory are considered bio-pore rich treatments because they are expected to

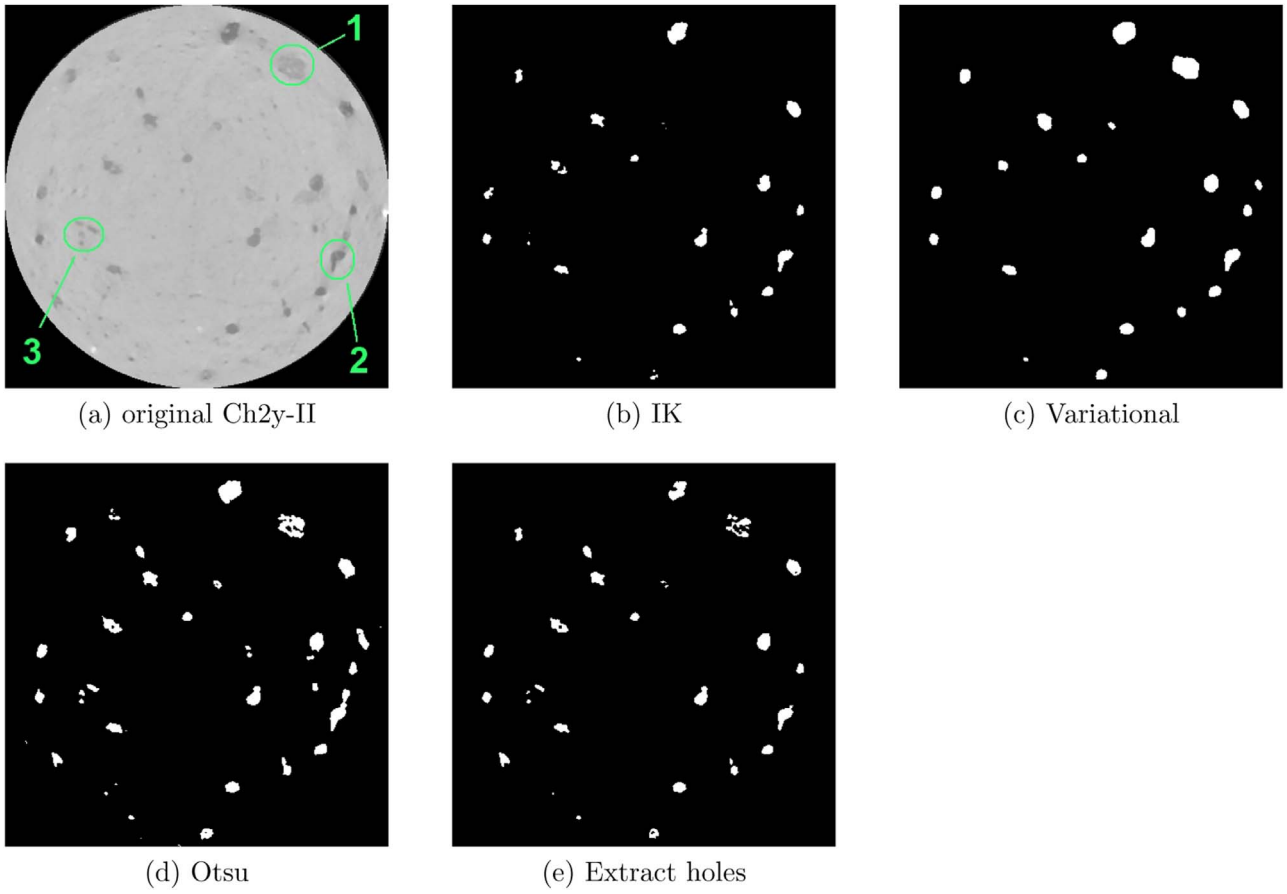

Fig. 3. Ch2y-II: Slice 200 perpendicular to the z-axis. (a)original Ch2y-II (b)IK (c)Variational (d)Otsu (e)Extract holes.

generate bio-pores (with larger diameters) in the subsoil by their specific root systems. The data set Ch2y-II is visualized in Fig. 1(a). Moreover, we applied the methods to two simulated bio-pore systems. The latter are realizations of a generalization of the Altendorf-Jeulin model for stochastic fiber systems (Altendorf and Jeulin, 2011) that allows for branching. The gray value distributions in these data sets are adapted from those observed in the real data sets. A simulated example set is depicted in Fig. 1(b).

4.2. Parameters

The variational segmentation algorithm does not require a pre-processing of the data since the noise and illumination removal is inherent in the method. The parameters for the real-world data are $\varepsilon = 0.2$, $c = \pm 0.03$ and $\mu = 6$. (If τ is too small when c=0, set c=0.03, and if τ is too big when c=0, set $c = -0.03$.) For the simulated data ε is changed to 0.01.

For the histogram based selection of the thresholds for IK, in total about 100 regions of interest (ROI) were extracted from the sample to include a sufficient fraction of bio-pore volume. The gray value histogram for those ROI are then smoothened by a local mean filter, resulting in two local maxima: A small one for the bio-pores and a larger one for the soil. For each ROI we derive a local T_0 as the first maximum and determine the global T_0 ($T_0 \in [133, 152]$) as the median over all local values. $T_1 \in [156, 173]$ is chosen as described in Pagenkemper et al. (2013). In a post-processing step all objects

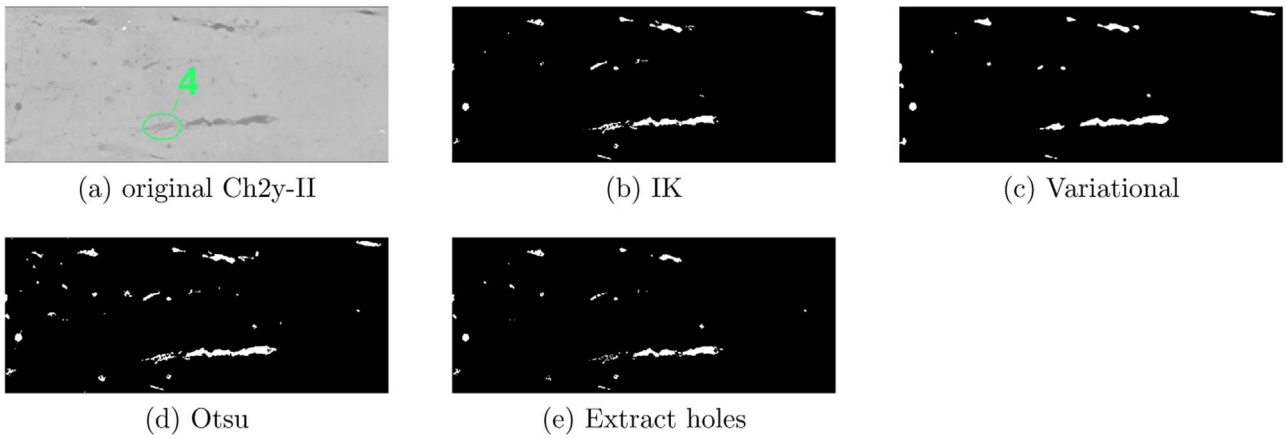

Fig. 4. Ch2y-II: Slice 180 parallel to the z-axis. (a)original Ch2y-II (b)IK (c)Variational (d)Otsu (e)Extract holes.

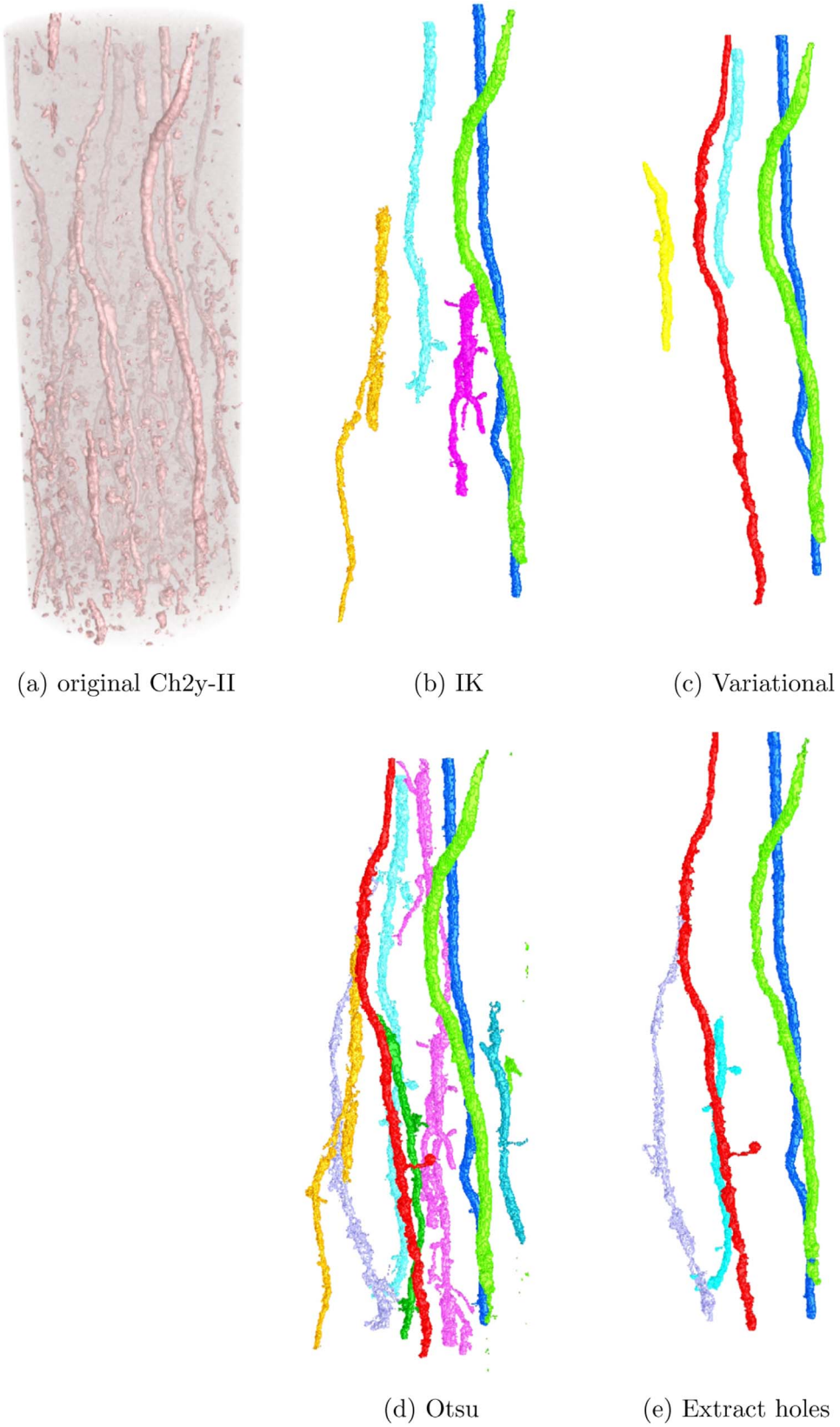

Fig. 5. Volume renderings of the segmented pores on Ch2y-II larger than 75 554 voxels – 9 pores for Otsu's threshold, 5 pores for all other methods. (a)original Ch2y-II (b)IK (c) Variational (d)Otsu (e)Extract holes.

smaller than 800 voxels were removed.

Otsu's thresholds in the corrected images, restricted to the cylindrical sample, are in the range [160, 174]. The result of the extract holes transform was thresholded by Otsu's method too – in that case 7-15.

Before applying extract holes, the side of the cylindrical sample is set to foreground to avoid edge effects.

4.3. Visual comparison

Visual impression suggests that the variational method yields the smoothest pores and keeps thin pores connected, see Fig. 2 for volume renderings as well as Figs. 3 and 4 showing 2D slices through the 3D images. Moreover, it also detects pores of intermediate gray value. Compare in particular the large but low contrast pores marked by 1 in Fig. 3 and marked by 4 in Fig. 4. The first one is completely missing in the IK segmentation, see Fig. 3(b), and very ragged in the extract holes results, see Fig. 3(e). Both IK and the variational method lose some small pores (right side of the slices, e.g. those marked by 3 in Fig. 3). Otsu's threshold and extract holes retain this detail, but the first one unites erroneously two pores (marked by 2 in Fig. 3). Extract holes is here more accurate. Compared to the other segmentations, it loses some of the pores when the small regions are removed. In general, Otsu's threshold and extract holes segment more small details but at the price of a much rougher surface....

Visual inspection of the largest pores in Ch2y-II in Fig. 5 singles out Otsu's threshold as this approach creates 9 pores above the volume threshold whereas the other methods have only 5 pores of this size. This is most likely due to the observed over segmentation which artificially connects pores..

4.4. Quantitative analysis

Table 1 shows that in general Extract holes followed by removal of small connected components segments the smallest pore volume while Otsu's threshold detects the largest. In accordance with the purely visual findings, the variational method clearly results in the smoothest pore system: It yields the smallest pore surface for all real samples. The strong connectivity of the pores segmented by the variational method becomes apparent in the mean chord lengths in z-direction – for the variational method this value is nearly twice as large as for the other methods, see Table 2.

Labelling of the pores and subsequent statistical analysis of the thus obtained image objects underlines the above findings. Table 3 below shows for several sizes the number of connected components. For the two simulated data sets, these numbers are compared to the truth, too. Extract holes never yields the right number of large pores, whereas all other methods come close to the true one for pores larger than 2000 and 5000 voxels, respectively.

Comparison to the ground truth for the two simulated bio-pore systems is clearly in favor of the variational method. Due to the extremely low volume fraction, percentage of misclassified voxels with respect to all voxels is not meaningful. Instead, the number of misclassified voxels is related to the total number of foreground (bio-pore) voxels. This yields the results summarized in Table 4. The variational method is clearly the one reproducing the true structures best. Nevertheless, it still classifies a quarter of the bio-pore pixels wrongly leaving a lot of space for improvement.

5. Conclusions

In this paper, we compared several approaches for segmenting bio-pores in 3D images of soil samples obtained by computed tomography. We proposed a variational alternative to the usually applied double thresholding methods (Oh and Lindquist, 1999; Pagenkemper et al., 2013; Schlüter et al., 2010).

The novel variational approach features well-connected smooth pores while not detecting smaller or shallower pores. This can be an advantage in cases where the main bio-pores network is of interest and where infillings (e.g. excrements of earthworms) would result in losing pore connections as observed for the other thresholding methods. Moreover, the smooth surface eases subsequent skeletonization as artificial branches due to local surface roughness are avoided.

Global thresholding preceded by a thorough shading correction yields a sound result as well. The observed tendency to over segmentation can be avoided by the morphological extract holes operation. These two methods have the significant advantage that the user does not have to choose critical parameters: The threshold is derived directly from the image's gray value histogram by Otsu's method. For the shading correction, gray value means in properly chosen regions suffice. Just when removing small connected components during the post-processing step, the user critically influences the result.

The final decision for one or the other method should thus rather depends on the final goal after segmentation.

Acknowledgements

GS and KS were partly supported by the German Federal Ministry of Education and Research through project 05M13 (AniS). The authors thank Prakash Easwaran for the simulated bio-pore systems.

Appendix A. Supplementary data

Supplementary data associated with this article can be found in the online version at http://dx.doi.org/10.1016/j.cageo.2016.09.013.

Table 1
Volume fraction and surface area of the segmented pore systems. True volume fraction of sim1 is 0.47%, of sim2 0.76%. The true surface areas are 0.054 m^2 and 0.074 m^2, for sim1 and sim2, respectively.

	Volume fraction [%]				Surface area [m^2]			
Sample	IK	Variational method	Otsu	Extract holes	IK	Variational method	Otsu	Extract holes
Ch2y-II	1.63	2.14	2.63	1.84	0.193	0.178	0.370	0.284
Fe1y-II	1.61	1.50	2.90	1.86	0.256	0.110	0.558	0.377
Af2y-I	1.24	1.39	2.46	1.18	0.167	0.070	0.443	0.303
Af2y-II	1.14	0.82	2.96	1.26	0.138	0.048	0.515	0.294
Sim1	0.79	0.55	0.81	0.63	0.102	0.049	0.103	0.085
Sim2	1.10	0.94	1.12	0.63	0.117	0.069	0.119	0.079
After removal of all objects smaller than 800 voxels								
Ch2y-II	1.62	2.08	2.31	1.55	0.191	0.167	0.263	0.189
Fe1y-II	1.31	1.47	2.19	1.30	0.157	0.104	0.296	0.170
Af2y-I	1.09	1.39	1.92	0.62	0.120	0.070	0.249	0.098
Af2y-II	1.03	0.81	2.45	0.80	0.103	0.048	0.320	0.120
Sim1	0.60	0.55	0.60	0.43	0.059	0.049	0.059	0.042
Sim2	0.91	0.94	0.92	0.43	0.075	0.069	0.075	0.034

Table 2
Mean chord lengths in *z*-direction.

	Mean chord length in *z*-direction [mm] after removal of all objects smaller than 800 voxels				
Sample	IK	Variational method	Otsu	Extract holes	True
Ch2y-II	5.37	10.07	5.31	5.14	
Fe1y-II	4.87	9.90	3.88	4.01	
Af2y-I	4.34	9.61	3.31	2.74	
Af2y-II	5.52	12.39	3.47	3.09	
Sim1	10.15	15.79	10.10	9.11	13.29
Sim2	13.39	18.23	13.49	12.22	15.50

Table 3
Joint connectivity and pore size analysis.

	Number of remaining pores after removal of all objects smaller than 800 voxels				
Sample	IK	Variational method	Otsu	Extract holes	True
Ch2y-II	222	214	263	266	
Fe1y-II	232	199	332	260	
Af2y-I	118	59	189	203	
Af2y-II	103	62	194	158	
Sim1	63	12	66	54	11
Sim2	46	17	45	31	11
	After removal of all objects smaller than 2000 voxels				
Ch2y-II	104	128	122	114	
Fe1y-II	109	118	141	122	
Af2y-I	47	40	71	85	
Af2y-II	57	52	75	79	
Sim1	13	11	13	6	11
Sim2	14	14	14	5	10
	After removal of all objects smaller than 5000 voxels				
Ch2y-II	60	73	62	65	
Fe1y-II	55	66	70	61	
Af2y-I	18	26	27	32	
Af2y-II	31	33	30	29	
Sim1	7	8	7	4	9
Sim2	11	10	11	3	10

Table 4
Fraction of misclassified voxels w.r.t. number of true foreground voxels.

Sample	IK	Variational method	Otsu	Extract holes
Sim1	68%	27%	75%	92%
Sim2	44%	25%	51%	90%
	after removal of all objects smaller than 800 voxels			
Sim1	34%	27%	41%	58%
Sim2	24%	25%	31%	70%

References

Altendorf, H., Jeulin, D., 2011. Random-walk-based stochastic modeling of three-dimensional fiber systems. Phys. Rev. E 83, 041804.

Boyd, S., Parikh, N., Chu, E., Peleato, B., Eckstein, J., 2011. Distributed optimization and statistical learning via the alternating direction method of multipliers. Found. Trends Mach. Learn. 3 (1), 101–122.

Cai, X., Steidl, G., 2013. Multiclass Segmentation by Iterated ROF Thresholding, EMMCVPR(2013). Lect. Notes Comput. Sci. 8081, 237–250.

Chambolle, A., Caselles, V., Novaga, M., Cremers, D., Pock, T., 2010. An Introduction to Total Variation for Image Analysis. Theoretical Foundations and Numerical Methods for Sparse Recovery, De Gruyter, vol. 9, pp. 263–340.

Chambolle, A., Pock, T., 2011. A first-order primal-dual algorithm for convex problems with applications to imaging. J. Math. Imaging Vis. 40 (1), 120–145.

Chan, T.F., Vese, L.A., 2001. Active contours without edges. IEEE Trans. Image Process. 10, 266–277.

Fraunhofer ITWM, 2005. Department of Image Processing, MAVI–Modular Algorithms for Volume Images ⟨http://www.mavi-3d.de⟩.

Fraunhofer ITWM, 2009. Department of Image Processing. ToolIP – tool for image processing ⟨http://www.itwm.fraunhofer.de/toolip⟩.

Fraunhofer ITWM, 2013. Department of Image Processing. MAVIkit –MAVI toolbox for ToolIP ⟨http://www.itwm.fraunhofer.de/toolip⟩.

Gabay, D., 1983. Applications of the method of multipliers to variational inequalities. In: Fortin, M., Glowinski, R., (Eds.), Augmented Lagrangian Methods: Applications to the Solution of Boundary Value Problems, IX:299–340, North-Holland, Amsterdam, 1983.

Iassonov, P., Gebrenegus, T., Tuller, M., 2009. Segmentation of X-ray computed tomography images of porous materials: a crucial step for characterization and quantitative analysis of pore structures. Water Resour. Res. 45, W09415.

Kappes, J.H., Andres, B., Hamprecht, F.A., Schnörr, C., Nowozin, S., Batra, D., Kim, S., Kausler, B.X., Kröger, T., Lellmann, J., et al., 2015. A comparative study of modern inference techniques for structured discrete energy minimization problems. Int. J. Comput. Vis. 115 (2), 155–184.

Lellmann, J., Kappes, J., Yuan, J., Becker, F., Schnörr, C., 2009. Convex multi-class image labeling with simplex-constrained total variation. In: Tai, X.-C., Morken, K., Lysaker, M., Lie, K.-A. (Eds.), Scale Space and Variational Methods, LNCS 5567. Springer, 150–162.

Mooney, S., 2002. Three-dimensional visualization and quantification of soil macroporosity and water flow patterns using computed tomography. Soil Use Manag. 18, 142–151.

Mumford, D., Shah, J., 1989. Optimal approximation by piecewise smooth functions and associated variational problems. Commun. Pure Appl. Math. 42, 577–685.

Nikolova, M., Esedoglu, S., Chan, T.F., 2006. Algorithms for finding global minimizers of image segmentation and denoising models. SIAM J. Appl. Math. 66 (5), 1632–1648.

Oh, W., Lindquist, W.B., 1999. Image Thresholding by Indicator Kriging. IEEE Trans. Pattern Anal. Mach. Intell. 21 (6), 590–602.

Otsu, N., 1979. A threshold selection method from gray level histograms. IEEE Trans. Syst. Man Cybern. 9, 62–66.

Pagenkemper, S., Peth, S., Puschmann, D., Horn, R., 2013. Effects of Root-Induced Biopores on Pore Space Architecture Investigated with Industrial X-Ray Computed Tomography. In: Anderson, S.H., Hopmans, J.W., (Eds.), Soil - Water - Root Processes:, Soil Science Society of America, Madison, pp. 69–96.

Pock, J.T., Chambolle, A., Cremers, D., Bischof, H., 2009. A convex relaxation approach for computing minimal partitions. In: Proceedings of IEEE Conference on Computer Vision and Pattern Recognition, CVPR2009, pp. 810–817.

Rudin, L.I., Osher, S., Fatemi, E., 1992. Nonlinear total variation based noise removal algorithms. Physica D. 60, 259–268.

Schlüter, S., Sheppard, A., Brown, K., Wildenschild, D., 2014. Image processing of multiphase images obtained via X-ray microtomography: a review. Water Resour. Res. 50 (4), 3615–3639.

Shafei, B., Steidl, G., 2012. Segmentation of images with separating layers by fuzzy c-means and convex optimization. J. Vis. Commun. Image Represent. 23, 611–621.

Tracy, S., Roberts, J., Black, C., McNeill, A., Davidson, R., Mooney, S., 2010. The X-factor: visualizing undisturbed root architecture in soils using X-ray computed tomography. J. Exp. Bot. 61, 311–313.

Schlüter, S., Weller, U., Vogel, H.-J., 2010. Segmentation of x-ray microtomography images of soil using gradient masks. Comput. Geosci. 36 (10), 1246–1251.

Soille, P., 1999. Morphological Image Analysis. Springer, Berlin, Heidelberg, New York.

Vogel, H., Kretzschmar, A., 1996. Topological characterization of pore space in soil-sample preparation and digital image-processing. Geoderma 73 (1), 23–38.

Zach, C., Gallup, D., Frahm, J.-M., Niethammer, M., 2008. Fast global labeling for real-time stereo using multiple plane sweeps. Vision, Modeling, and Visualization Workshop.